# A dynamic model for the Lagrangian-averaged Navier-Stokes-$\alpha$ equations

Hongwu Zhao and Kamran Mohseni[a)]
*Aerospace Engineering Sciences, University of Colorado, 107-81, Boulder, Colorado 80309-0429*

(Received 27 August 2004; accepted 17 May 2005; published online 6 July 2005)

A *dynamic* procedure for the Lagrangian-averaged Navier-Stokes-$\alpha$ (LANS-$\alpha$) equations is developed where the variation in the parameter $\alpha$ in the direction of anisotropy is determined in a self-consistent way from the data contained in the simulation itself. In order to derive this model, the incompressible Navier-Stokes equations are Helmholtz filtered at the grid and test filter levels. A Germano-type identity is derived by comparing the filtered subgrid-scale stress terms with those given in the LANS-$\alpha$ equations. Assuming constant $\alpha$ in homogenous directions of the flow and averaging in these directions result in a nonlinear equation for the parameter $\alpha$, which determines the variation of $\alpha$ in the nonhomogeneous directions or in time. Consequently, the parameter $\alpha$ is calculated during the simulation instead of a predefined value. The dynamic model is initially tested in forced and decaying isotropic turbulent flows where $\alpha$ is constant in space but it is allowed to vary in time. It is observed that by using the dynamic LANS-$\alpha$ procedure a more accurate simulation of the isotropic homogeneous turbulence is achieved. The energy spectra and the total kinetic-energy decay are captured more accurately as compared with the LANS-$\alpha$ simulations using a fixed $\alpha$. In order to evaluate the applicability of the dynamic LANS-$\alpha$ model in anisotropic turbulence, *a priori* test of a turbulent channel flow is performed. It is found that the parameter $\alpha$ changes in the wall normal direction. Near a solid wall, the length scale $\alpha$ is seen to depend on the distance from the wall with a vanishing value at the wall. On the other hand, away from the wall, where the turbulence is more isotropic, $\alpha$ approaches an almost constant value. Furthermore, the behavior of the subgrid-scale stresses in the near-wall region is captured accurately by the dynamic LANS-$\alpha$ model. The dynamic LANS-$\alpha$ model has the potential to extend the applicability of the LANS-$\alpha$ equations to more complicated anisotropic flows. © *2005 American Institute of Physics*. [DOI: 10.1063/1.1965166]

## I. INTRODUCTION

Turbulent flows play an important role in many areas of engineering fluid mechanics as well as atmospheric and oceanic flows. Accurate simulation of a turbulent flow requires the energetics of the large-scale energy containing eddies, dissipative small scales, and interscale interactions to be accounted for. In direct numerical simulations (DNSs) all the involved scales are directly calculated. DNS is believed to provide the most comprehensive representation of the governing equations of fluid flows; the so-called Navier-Stokes (NS) equations. Owing to the very high Reynolds numbers encountered in most problems of interest, the disparity between the large scales and small scales, which represents the computational size of the problem, rapidly grows with the Reynolds number. Consequently, DNS can resolve only a small fraction of the turbulent activity for high Reynolds number flows.

While the direct numerical simulation of most engineering flows seems unlikely in the near future, turbulence modeling could provide qualitative and in some cases quantitative measures for many applications. Large eddy simulations (LESs) and the Reynolds-averaged Navier-Stokes (RANS) equations are among the numerical techniques to reduce the computational intensity of turbulent calculations. In LES, the dynamics of the large turbulence length scales are simulated accurately and the small scales are modeled. The vast majority of contemporary LESs make use of eddy-viscosity-based subgrid-scale (SGS) models in conjunction with the spatially averaged (filtered) Navier-Stokes equations. In this approach, the effect of the unresolved turbulence is modeled as an effective increase in the molecular viscosity. On the other hand, RANS models are obtained by time averaging the Navier-Stokes equations. In this case most of the unsteadiness is averaged out. Consequently, the time mean quantities are calculated while the faster scale dynamics are modeled. RANS simulations are often more affordable than LES, however, their accuracy is somewhat limited in many applications.[1]

More recently, Holm, Marsden, and Ratiu[2] introduced a Lagrangian averaging technique for the mean motion of ideal incompressible flows. Figure 1 contrasts the derivation of LES, RANS, and the Lagrangian-averaged Navier-Stokes-$\alpha$ (LANS-$\alpha$) equations. Unlike the traditional averaging or filtering approach used for both RANS and LES, where the Navier-Stokes equations are averaged or spatially filtered, the Lagrangian averaging approach is based on averaging at the level of the variational principle. In the isotropic Lagrangian-averaged Euler-$\alpha$ (LAE-$\alpha$) equations, fluctuations smaller than a specified scale $\alpha$ are averaged at the level of the flow maps.[3] Mean fluid dynamics are derived by

[a)]Author to whom correspondence should be addressed. Telephone: (303) 492 0286. Fax: (303) 492 7881. Electronic mail: mohseni@colorado.edu

 

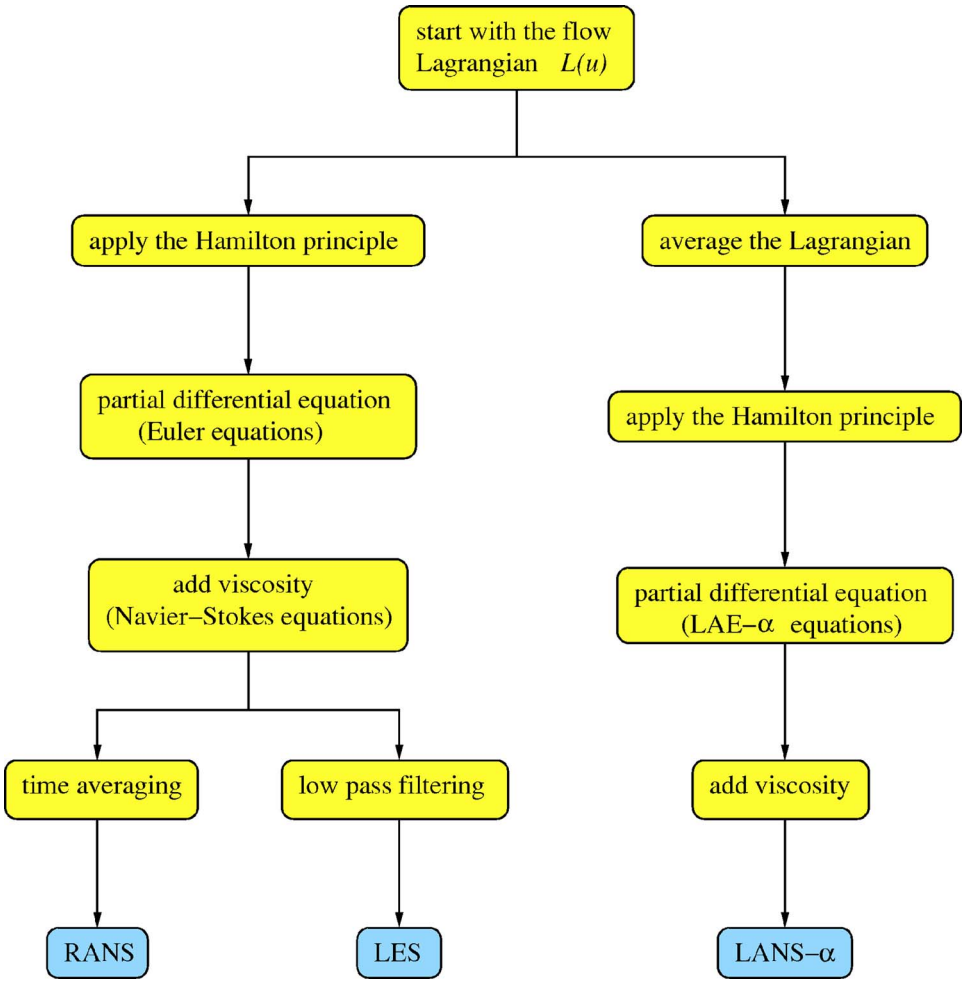


FIG. 1. Derivation of the averaged flow equations.

applying an averaging procedure to the action principle of the Euler equations. As shown in Fig. 1, both the Euler and the Navier-Stokes equations can be derived in this manner (see Marsden and Ratiu[4] for a variational derivation of the Euler equations). The usual RANS or LES equations are then obtained through the subsequent application of either a temporal or spatial average. The critical difference with the Lagrangian averaging procedure is that the Lagrangian (kinetic energy minus potential energy) is averaged *prior* to the application of the Hamilton principle and a closure assumption is applied at this stage. This procedure results in either the LAE-$\alpha$ [In this nomenclature, $\alpha$ is used to denote the filtering scale (i.e., the simulation faithfully represents motions on a scale larger than $\alpha$)] or the LANS-$\alpha$, depending on whether or not a random-walk component is added in order to produce a true molecular diffusion term. Since the Hamilton principle is applied after the Lagrangian averaging is performed, *all* the geometrical properties (e.g., invariants) of the inviscid dynamics are retained even in the presence of the model terms which arise from the closure assumption.[2,5,6] For instance, LAE equations posses a Kelvin circulation theorem. Thus it is potentially possible to model the transfer of energy to the unresolved scales without an incorrect attenuation of quantities such as resolved circulation. This is an important distinction for many engineering and geophysical flows where the accurate prediction of circulation is highly desirable.

Numerical simulations by Chen, Holm, Margoin, and Zhang[7] and Mohseni Kosovic, Shkoller, and Marsden[8] showed the capability of the LANS-$\alpha$ equations in simulating isotropic homogenous turbulence. However, most engineering and geophysical flows of interest are often anisotropic. For example, due to rapid damping of turbulent fluctuations in the vicinity of a wall, the application of the isotropic LANS-$\alpha$ equations with a constant $\alpha$ is not appropriate for long-term calculations. In order to capture the correct behavior in such systems the parameter $\alpha$ must be spatially or/and temporally varied in the direction of anisotropy,[9] i.e., wall normal direction. There has been some attempt (with limited success) in order to remedy this problem. A successful *dynamic* LANS-$\alpha$ model is yet to be formulated and tested. There are at least two approaches to anisotropy in the LANS-$\alpha$ equations:

(i) to derive a set of *anisotropic* LANS-$\alpha$ equations (see alternative derivations in Refs. 6 and 10 and
(ii) use the isotropic LANS-$\alpha$ equations, but with a variable $\alpha$ to compensate for the anisotropy.

At this point much more work must be done on the aniso-

tropic LANS-$\alpha$ equations before they can be applied to practical problems. The second approach listed above is what will be explored in this study.

This paper is organized as follows: The isotropic LANS-$\alpha$ equations and some of their main features are summarized in Sec. II. A dynamic LANS-$\alpha$ approach is proposed in Sec. III where the variation in the parameter $\alpha$ in the direction of anisotropy is determined in a self-consistent way from the data contained in the simulation itself. Our approach will be developed in the same spirit as the dynamic modeling procedure for conventional LES (Refs. 11–14) which has achieved widespread use as very effective means of estimating model parameters as a function of space and time as the simulation progresses. The incompressible Navier-Stokes equations are Helmholtz filtered at the grid and test filter levels. A Germano-type identity is derived by comparing the filtered subgrid-scale stress terms with those given in the LANS-$\alpha$ equations. Considering a constant value of $\alpha$ and averaging in the homogenous directions of the flow result in a nonlinear equation for the parameter $\alpha$, which determines the variation of $\alpha$ in the nonhomogeneous directions or time. This nonlinear equation is solved by an iterative technique. Consequently, the parameter $\alpha$ is calculated during the simulation instead of a fixed and predefined value.

Numerical techniques for simulating the dynamic LANS-$\alpha$ model in this study are described in Sec. IV. The performance of the dynamic LANS-$\alpha$ model in simulating forced and decaying isotropic homogeneous turbulent flows is considered in Sec. V. In statistically equilibrated forced turbulence, the parameter $\alpha$ should remain constant in time and space. In decaying isotropic turbulence, the parameter $\alpha$ could change in time as the integral scales of the turbulent flow change. In order to demonstrate the applicability of the dynamic LANS-$\alpha$ model of this study in anisotropic flows, *a priori* test of turbulent channel flows is also performed in Sec. V. The concluding results are presented in Sec. VI.

## II. THE ISOTROPIC LANS-$\alpha$ EQUATIONS

The incompressible isotropic LANS-$\alpha$ equations for the large-scale velocity $u$ are given by (see Ref. 2 for a derivation)

$$\frac{\partial u}{\partial t} + (u \cdot \nabla) u = -\nabla p + \frac{1}{\mathrm{Re}} \Delta u + \nabla \cdot \tau(u), \tag{1}$$

$$\nabla \cdot u = 0, \tag{2}$$

where $\tau(u)$ is the subgrid stress tensor defined as[3]

$$\tau(u) = -\alpha^2 (1 - \alpha^2 \Delta)^{-1} [\nabla u \cdot \nabla u^T - \nabla u^T \cdot \nabla u + \nabla u \cdot \nabla u + \nabla u^T \cdot \nabla u^T]. \tag{3}$$

The subgrid-scale stress $\tau(u)$ is, in fact, the momentum flux of the large scales caused by the action of smaller, unresolved scales. Here $\alpha$ is a constant length scale introduced during the averaging process. Note that for vanishing parameter $\alpha$ the NS equations will be recovered.

The LANS-$\alpha$ equations can be represented equivalently by

$$\frac{\partial v}{\partial t} + (u \cdot \nabla) v + v_j \nabla u_j = -\nabla P + \frac{1}{\mathrm{Re}} \Delta v, \tag{4}$$

where $v_i$ is defined as $v = u - \alpha^2 \Delta u$. The modified pressure $P$ in these equations is determined, as usual, from the incompressibility conditions: $\nabla \cdot u = 0$ and $\nabla \cdot v = 0$.

One interpretation for Eq. (1) is that it is obtained by averaging the Euler equations in Lagrangian representation over rapid fluctuations whose scale are of order $\alpha$. In this respect, one can show that the Lagrangian-averaged Euler equations can be regarded as geodesic equations for the $H^1$ metric on the volume preserving diffeomorphism group, as what Arnold[15] did with the $L_2$ metric for the Euler equations. Note that in calculating the SGS stress $\tau(u)$ in Eq. (3) one needs to calculate the inverse of the Helmholtz operator $(1 - \alpha^2 \Delta)$, which implies the need to solve a Poisson equation. While efficient numerical treatment of the Poisson equation, or its possible elimination through rational approximation will be a focus of a future publication, we note, in passing, that the inverse of the Helmholtz operator can be expanded in $\alpha$ to higher orders of the Laplacian operator as shown below:

$$(1 - \alpha^2 \Delta)^{-1} = 1 + \alpha^2 \Delta + \alpha^4 \Delta^2 + \cdots \quad \text{if } \alpha \lambda_{\max} < 1, \tag{5}$$

where $\lambda_{\max}$ is the highest eigenvalue of the discretized operator $\Delta$. It should be noted that in a periodic domain one can easily convert the equation

$$(1 - \alpha^2 \Delta)^{-1} v = u \tag{6}$$

$$\check{v} = \frac{1}{1 + \alpha^2 k^2} \check{u} \tag{7}$$

in Fourier space where $\check{(\cdot)}$ stands for variables in the Fourier space, and $k$ is the wavenumber. Now using the Taylor expansion on the right-hand side one can obtain

$$\frac{1}{1 + \alpha^2 k^2} = 1 - \alpha^2 k^2 + \alpha^4 k^4 - \cdots \quad \text{if } \alpha^2 k^2 < 1. \tag{8}$$

In the case of numerical discretization of $\Delta$ the convergence condition is reduced to $\alpha^2 k_{\max}^2 < 1$, where $k_{\max}$ is the highest wave mode captured in the simulation. Note that $\alpha$ is the cutoff scale of the Helmholtz inverse filter. Therefore, $1/\alpha$ is the highest wave mode captured accurately by the LANS-$\alpha$ model. The promise of the LANS-$\alpha$ equations is to capture the large scales ($< 1/\alpha$) accurately, while the small scales are modeled. To this end, the condition $\alpha^2 k^2 < 1$ must hold in any accurate simulation using the dynamic LANS-$\alpha$ equations. As a result, one can avoid solving a Poisson equation to invert the Helmholtz operator using the expansion (5).

It is interesting to note that the Lagrangian averaging technique preserves the Hamiltonian structure of the governing equations in the inviscid limit while the effects of small scales on the macroscopic features of large scale are taken into account in a conservative manner. The Hamiltonian and Lagrangian formulations of ideal fluids are both basic and useful. These formulations are part of a more general framework of *geometric mechanics*, which plays a vital role in the development of new continuum models suited for computa-

tion, as well as numerical algorithms that preserve structure at the discrete level. In the recent years the geometric approach to fluid mechanics has been quite successful. Geometrical methods provide a framework for the study of nonlinear stability,[16] variational integrators,[17,18] statistical equilibrium theory,[19–23] and many other interesting topics in fluid dynamics. The Lagrangian-averaged Navier-Stokes-$\alpha$ uses ideas from geometric mechanics and offers a theoretically and computationally attractive approach to the turbulence closure problem.

## III. DERIVATION OF A DYNAMIC LANS-$\alpha$ MODEL

The LANS-$\alpha$ equations for the large-scale velocity $u$ are given by Eq. (1), where $\tau(u)$ is the subgrid stress tensor defined in (3). This set of equations for $\alpha$ is similar to the grid-filtered equation in the dynamic LES. In analogy with the dynamic LES one can obtain an equation for the filtering length scale $\alpha$ by filtering the Navier-Stokes equations,

$$\frac{\partial u_i}{\partial t} + u_j \frac{\partial u_i}{\partial x_j} = -\frac{\partial p}{\partial x_i} + \frac{1}{\mathrm{Re}} \frac{\partial^2 u_i}{\partial x_j \partial x_j}, \tag{9}$$

with the Helmholtz-related filters,

$$\bar{u} = (1 - \alpha^2 \Delta)^{-1} u, \quad \text{grid filter}, \tag{10}$$

$$\hat{\bar{u}} = (1 - \hat{\alpha}^2 \Delta)^{-1} (1 - \alpha^2 \Delta)^{-1} u, \quad \text{test filter}, \tag{11}$$

to obtain

$$\frac{\partial \bar{u}_i}{\partial t} + \frac{\partial \bar{u}_i \bar{u}_j}{\partial x_j} = -\frac{\partial \bar{p}}{\partial x_i} + \frac{1}{\mathrm{Re}} \frac{\partial^2 \bar{u}_i}{\partial x_j \partial x_j} - \frac{\partial \tau_{ij}}{\partial x_j}, \tag{12}$$

$$\frac{\partial \hat{\bar{u}}_i}{\partial t} + \frac{\partial \hat{\bar{u}}_i \hat{\bar{u}}_j}{\partial x_j} = -\frac{\partial \hat{\bar{p}}}{\partial x_i} + \frac{1}{\mathrm{Re}} \frac{\partial^2 \hat{\bar{u}}_i}{\partial x_j \partial x_j} - \frac{\partial T_{ij}}{\partial x_j}, \tag{13}$$

where

$$\tau_{ij} = \overline{u_i u_j} - \bar{u}_i \bar{u}_j,$$

$$T_{ij} = \widehat{\overline{u_i u_j}} - \hat{\bar{u}}_i \hat{\bar{u}}_j.$$

Using an idea similar to the Germano identity,[11] we define

$$L_{ij} = T_{ij} - \hat{\tau}_{ij} = \widehat{\bar{u}_i \bar{u}_j} - \hat{\bar{u}}_i \hat{\bar{u}}_j, \tag{14}$$

where the subgrid-scale stresses under two filtering actions can be modeled by the LANS-$\alpha$ subgrid term in Eq. (3). Therefore,

$$\tau_{ij} = \alpha^2 (1 - \alpha^2 \Delta)^{-1} M_{ij}, \tag{15}$$

$$T_{ij} = \hat{\alpha}^2 (1 - \hat{\alpha}^2 \Delta)^{-1} N_{ij}, \tag{16}$$

where

$$M_{ij} = \frac{\partial \bar{u}_i}{\partial x_k} \frac{\partial \bar{u}_j}{\partial x_k} - \frac{\partial \bar{u}_k}{\partial x_i} \frac{\partial \bar{u}_k}{\partial x_j} + \frac{\partial \bar{u}_i}{\partial x_k} \frac{\partial \bar{u}_k}{\partial x_j} + \frac{\partial \bar{u}_j}{\partial x_k} \frac{\partial \bar{u}_k}{\partial x_i},$$

$$N_{ij} = \frac{\partial \hat{\bar{u}}_i}{\partial x_k} \frac{\partial \hat{\bar{u}}_j}{\partial x_k} - \frac{\partial \hat{\bar{u}}_k}{\partial x_i} \frac{\partial \hat{\bar{u}}_k}{\partial x_j} + \frac{\partial \hat{\bar{u}}_i}{\partial x_k} \frac{\partial \hat{\bar{u}}_k}{\partial x_j} + \frac{\partial \hat{\bar{u}}_j}{\partial x_k} \frac{\partial \hat{\bar{u}}_k}{\partial x_i}.$$

Combining Eqs. (14)–(16), one obtains

$$L_{ij} = \beta^2 \alpha^2 (1 - \beta^2 \alpha^2 \Delta)^{-1} N_{ij} - \alpha^2 (1 - \beta^2 \alpha^2 \Delta)^{-1} (1 - \alpha^2 \Delta)^{-1} M_{ij} \tag{17}$$

or

$$L_{ij} = \alpha^2 (\beta^2 \hat{N}_{ij} - \hat{\bar{M}}_{ij}), \tag{18}$$

where $\beta = \hat{\alpha}/\alpha$. Multiplying both sides of the above equation by $S_{ij}$ yields

$$L_{ij} S_{ij} = \alpha^2 (\beta^2 \hat{N}_{ij} - \hat{\bar{M}}_{ij}) S_{ij}. \tag{19}$$

Taking spatial averaging of both sides of the above equation in homogenous directions, one obtains

$$\alpha^2 = \frac{\langle L_{ij} S_{ij} \rangle}{\langle (\beta^2 \hat{N}_{ij} - \hat{\bar{M}}_{ij}) S_{ij} \rangle}, \tag{20}$$

where

$$S_{ij} = \frac{1}{2} \left( \frac{\partial \bar{u}_i}{\partial x_j} + \frac{\partial \bar{u}_j}{\partial x_i} \right).$$

The denominator in Eq. (20) could approach zero, where it creates a singularity. In dynamic LES, Lilly[24] used a least square approach to eliminate the singularity in Germano's model. By a similar least-square approach a nonlinear equation for $\alpha$ could be found as

$$\alpha^2 = F(\alpha) = \frac{\langle L_{ij} (\beta^2 \hat{N}_{ij} - \hat{\bar{M}}_{ij}) \rangle}{\langle (\beta^2 \hat{N}_{ij} - \hat{\bar{M}}_{ij}) (\beta^2 \hat{N}_{ij} - \hat{\bar{M}}_{ij}) \rangle}, \tag{21}$$

which does not have the singularity problem as in Eq. (20). This is a nonlinear equation for $\alpha$. All the quantities in Eq. (21) can be calculated during a LANS-$\alpha$ simulation. Therefore, Eq. (21) provides a nonlinear equation for dynamically calculating the value of $\alpha$ during the simulation.

At this point the potential values for the free parameter $\beta$ are required. Writing the grid and test filters in Eqs. (10) and (11) in the Fourier space, one obtains

$$\breve{\bar{u}} = \frac{\breve{u}}{1 + \alpha^2 k^2}, \tag{22}$$

and

$$\breve{\hat{\bar{u}}} = \frac{\breve{u}}{(1 + \beta^2 \alpha^2 k^2)(1 + \alpha^2 k^2)} \approx \frac{\breve{u}}{1 + (\beta^2 + 1) \alpha^2 k^2} = \frac{\breve{u}}{1 + \tilde{\alpha}^2 k^2} \quad \text{as } k \to \infty, \tag{23}$$

where $\tilde{\alpha}$ corresponds to the filter scale for the test filter. Since $\tilde{\alpha} = \sqrt{1 + \beta^2} \alpha \geqslant \alpha$, one can realize that as long as $\beta > 0$, the test filter has a larger filter scale than the grid filter. Figure 2 shows the relative positions of the grid filter scale $\alpha$ and the test filter scale $\tilde{\alpha}$ on a schematic of the energy spectrum for a high Reynolds number flow. In order to accurately model the subgrid-scale stress, both the grid filter and the test filter scales must be located in the inertial subrange of the energy spectrum. It should be pointed out that the iterative calculation required in Eq. (21) does not require new flow

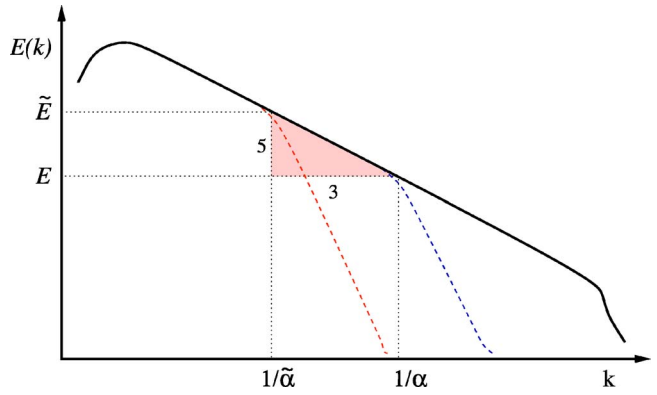


FIG. 2. The positions of grid and test filter scales on the turbulent kinetic-energy spectrum.

field calculations, and the iteration at each time step is carried out using the existing flow field at the same time step. Similar to the dynamic LES model, the present dynamic LANS-$\alpha$ model has a free parameter $\beta$, which is related to the characteristic length scale of the grid and test filters.

The dynamic $\alpha$ model given in Eq. (21) is designed to capture the length scale variations in space and time. Aside from the isotropic homogenous turbulent flows, it is well suited for anisotropic flows such as wall-bounded turbulence or mixing flow turbulence, where the turbulence length scales could change in space or in time. In cases where there are directions of homogeneity, such as the streamwise and spanwise directions in a channel flow, one can average the parameter $\alpha$ over the homogeneous directions. In a more general situation, we expect to replace the plane average, used in the channel flow, by an appropriate local spatial or time averaging scheme. For isotropic homogenous turbulence, $\alpha$ is regarded as a constant in space and changes only in time.

## IV. NUMERICAL METHOD

The dynamic procedure in this study is initially tested for forced and decaying isotropic turbulence where the parameter $\alpha$ is constant over the computational domain, but can vary in time. Furthermore, *a priori* test of the dynamic LANS-$\alpha$ procedure in a turbulent channel flow is investigated. In this section the numerical technique for solving the governing equations is summarized.

### A. Isotropic homogeneous turbulence

The computations are performed in a periodic cubic box of side $2\pi$. A standard parallel pesudospectral scheme with periodic boundary conditions is employed. The spatial derivatives are calculated in the Fourier domain, while the nonlinear convective terms are computed in the physical space. A fourth-order Runge-Kutta scheme is implemented to advance the flow field in time. The two-third rule is used in order to eliminate the aliasing errors. Therefore, the upper one-third of the wave modes are discarded at each stage of the Runge-Kutta scheme. The initial velocity field for each case was divergence free and constructed to generate an energy spectrum of the form

$$E(k) \sim k^4 \exp[-2(k/k_p)^2].$$

The value of $k_p$ corresponds to the peak in the energy spectrum. The initial pressure fluctuations were obtained from the solution of a Possion equation.

### B. Turbulent flow in a channel

The DNS data from del Álamo and Jiménez[25] are employed for the *a priori* test. The computational domain in this case, normalized based on the half-channel height, is spanned $8\pi$ in the streamwise and $4\pi$ in the spanwise directions. The spatial derivatives are calculated by the pesudospectral method in streamwise and spanwise directions and by the Chebychev-tau technique in the wall normal direction. Similar computational techniques have successfully been used for the DNS of channel flows by Kim, Moin, and Moser[26] and Moser, Kim, and Mansour.[27] Grid and test filters of Helmholtz types are applied in both streamwise and spanwise directions. A grid Helmholtz-type filter is applied in the wall normal direction at a fixed $\alpha$ value to filter the DNS data to a specific precision in this direction so that the SGS stresses get no oscillations in the near-wall region. No explicit test filters are applied in the wall normal direction. $\alpha$ is assumed to be constant in the homogenous directions, i.e., the streamwise and spanwise directions, in order to solve the nonlinear equation (20) and (21). These equations are solved by an iterative technique. Since both the mean flow and the flow perturbations vanish at the wall, singular behavior might occur in these equations. This can be easily fixed by starting the *a priori* test a few grid points away from the wall. In actual simulation of the dynamic LANS-$\alpha$ equations, one can explicitly put $\alpha$ to zero below in the immediate vicinity of a wall when the value of $\alpha$ drops below a threshold. The converged $\alpha$ values at each point are used as initial values for the iteration at the next grid layer.

## V. RESULTS AND DISCUSSIONS

The capabilities of the dynamic LANS-$\alpha$ model of the previous sections are examined in both isotropic and anisotropic turbulent flows. In isotropic homogeneous turbulence the parameter $\alpha$ is constant in space but allowed to vary in time. The results of the dynamic model are compared with the isotropic LANS-$\alpha$ simulations with a constant $\alpha$ and with the DNS data.

### A. Decaying isotropic homogenous turbulence simulations

The DNS of a decaying isotropic homogenous turbulence with initial Taylor Reynolds number of $\mathrm{Re}_\lambda = 72$ (corresponding to a computational Reynolds number $\mathrm{Re} = 300$) is performed to be used as a test case. The initial energy spectrum is peaked at $k_p = 4$. The isotropic LANS-$\alpha$ and the dynamic LANS-$\alpha$ simulations are calculated for both $64^3$ (corresponds to $42^3$ after dealiasing) and $48^3$ (corresponds to $32^3$ after dealiasing) resolutions, and direct numerical simulations are performed for $128^3$ (corresponds to $85^3$ after dealiasing). The eddy turn over time for this case is found to be $\tau = 0.9$. Figure 3 shows the time evolution of $\alpha$ for $\beta$

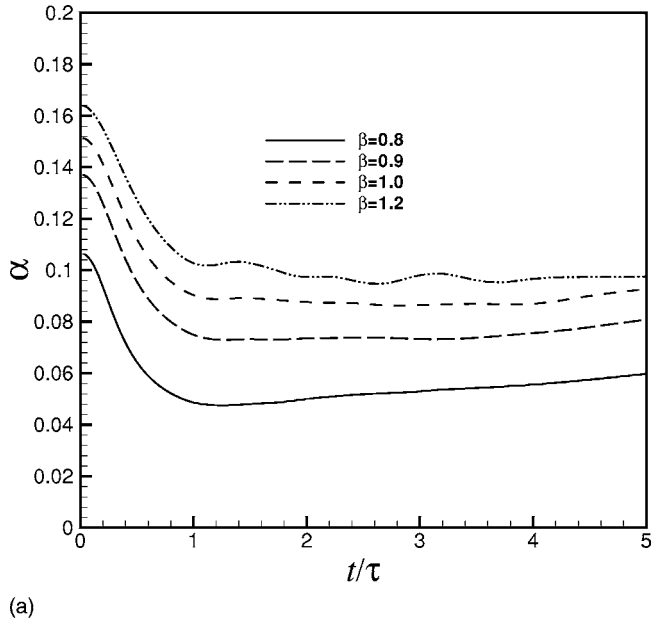


(a)

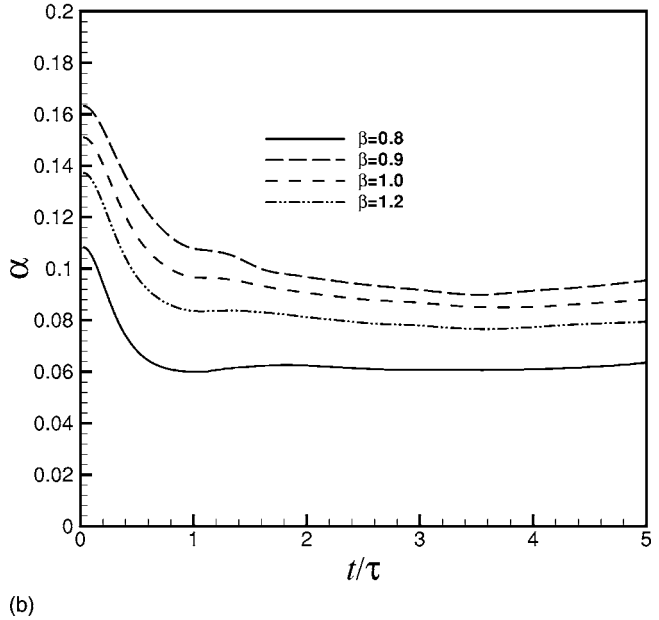


(b)

FIG. 3. Evolution of $\alpha$ at different $\beta$ for a decaying isotropic turbulence at $\mathrm{Re}_\lambda=72$ and $\tau=0.9$. Grid resolutions (a) $42^3$ and (b) $32^3$.

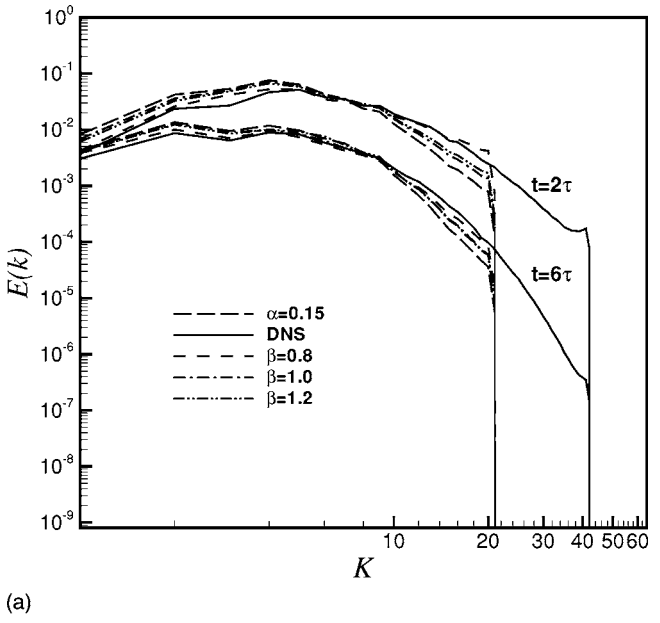


(a)

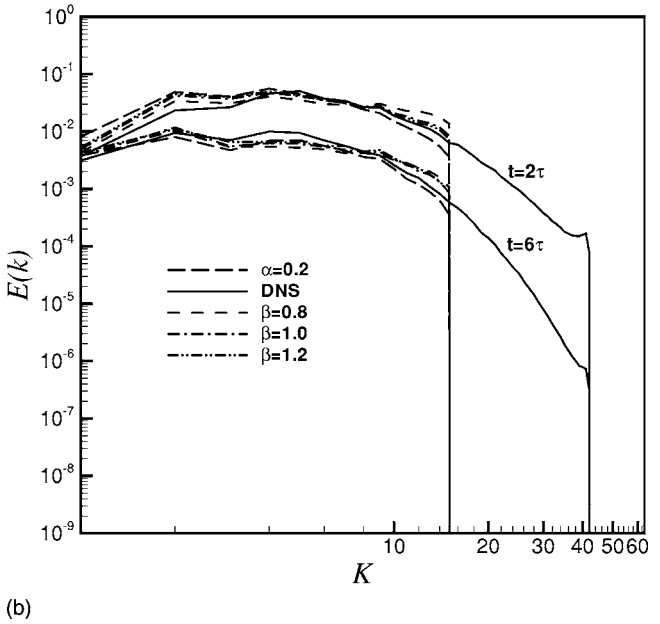


(b)

FIG. 4. Energy spectra of the DNS, dynamic LANS-$\alpha$, and LANS-$\alpha$ with fixed $\alpha$ simulations of a decaying isotropic turbulence at $\mathrm{Re}_\lambda=72$ and $\tau=0.9$. Grid resolutions (a) $42^3$ and (b) $32^3$.

$=0.8$, 0.9, 1, and 1.2. The values of $\alpha$ experience a sharp decrease from its initial value during the first eddy turn over time. However, it quickly settles down toward a much slower varying value. Slight changes in $\alpha$ value after the first eddy turn over time could be traced back to flattening of the energy spectrum as the turbulence decays.

The energy spectra at two different time instant are shown in Fig. 4, and the total kinetic-energy decay are shown in Fig. 5. While a slight dependency on the value of $\beta$ is observed, in general, the energy spectrum at various time and the total kinetic-energy decay are captured nicely. Mohseni, Kosovic, Shkoller, and Marsden[8] demonstrated that in order to accurately simulate a turbulent flow with the LANS-$\alpha$ equations, the value of $\alpha$ should be somewhere, perhaps one decade lower than the peak of the energy spectra toward the grid resolution. Careful considerations of Figs. 3 and 4 reveal that the dynamic LANS-$\alpha$ model of this study satisfies this criteria for all $\beta$ values. In general, one expects the value of $\alpha$ to be in the inertial range of the energy spectra in order to correctly capture the dynamics of the large scales. As illustrated in Figs. 4 and 5 it is evident that the dynamic LANS-$\alpha$ model provides a better estimate of the total kinetic-energy decay and the energy spectra over similar simulations with fixed $\alpha$ calculations.

### B. Forced isotropic homogenous turbulence simulations

Forced isotropic turbulence is one of the most idealized and extensively simulated turbulent flows. The numerical

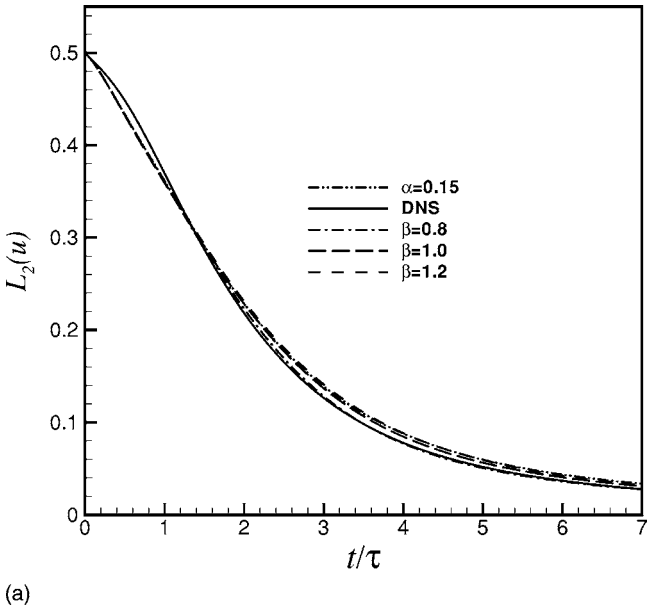


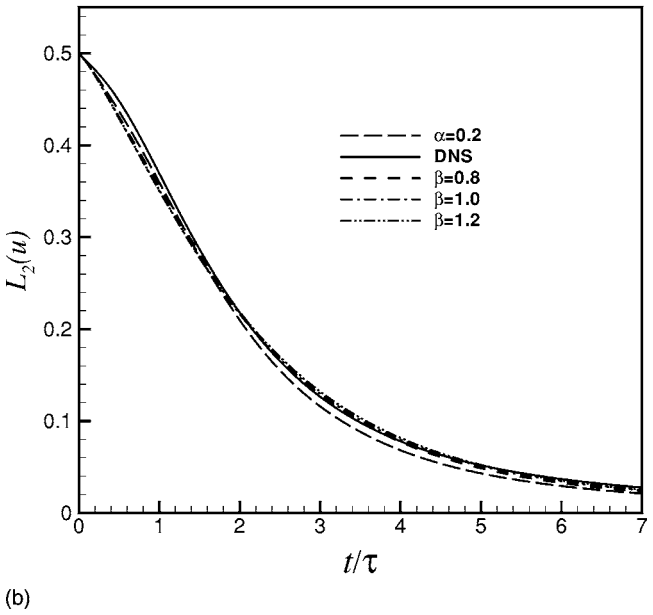


FIG. 5. Total kinetic-energy decay of the DNS, dynamic LANS-$\alpha$, and LANS-$\alpha$ with fixed $\alpha$ simulations of a decaying isotropic turbulence at $\mathrm{Re}_\lambda=72$ and $\tau=0.9$. Grid resolutions (a) $42^3$ and (b) $32^3$.

forcing of a turbulent flow is usually referred to the artificial addition of energy at the large scales in a numerical simulation. Statistical equilibrium is signified by the balance between the input of kinetic energy through the forcing and its output through the viscous dissipation. In this study, we adopted a forcing method used by Chen, Holm, Margoin, and Zhang[7] and Mohseni, Kosovic, Shkoller, and Marsden[8] where the wave modes in a spherical shell $|K|=k_0$ of certain width are forced in such a way that the forcing spectrum follows the Kolmogorov $-5/3$ scaling law, that is

$$\check{f}_i = \frac{\delta_0}{N}\frac{\check{u}_i}{\sqrt{\check{u}_k\check{u}_k^*}}k^{-5/3}. \tag{24}$$

Here $\check{f}_i$ and $\check{u}_i$ are the Fourier transforms of the forcing vector $f_i$ and velocity $u_i$, $N$ is the number of forced wave modes,

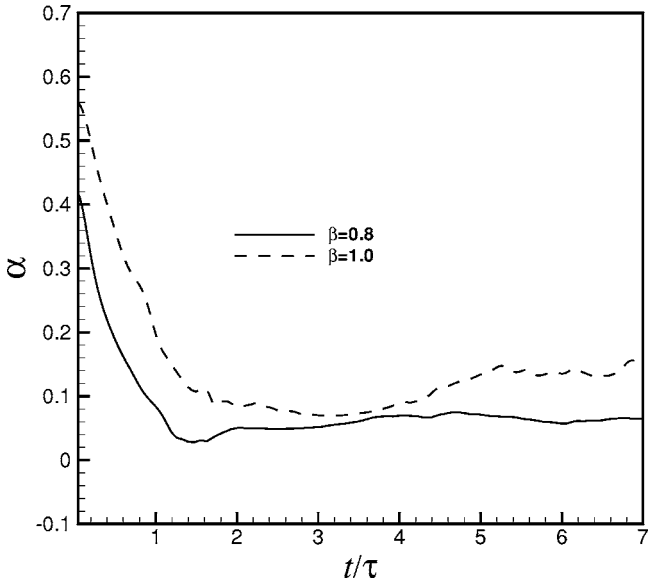


FIG. 6. Evolution of $\alpha$ at different $\beta$ in the forced turbulence case with $\mathrm{Re}_\lambda=415$ and $\tau=3.8$.

and $\delta$ controls the injection rate of energy at the large scales. This particular forcing technique enforces the energy cascade in the inertial range starting from first wave mode. In this simulations we choose $k_0=2$ and $\delta_0=0.1$. The initial Taylor Reynolds number is $\mathrm{Re}_\lambda=415$ and the initial energy spectrum is peaked at $k_p=1$, while the eddy turn over time is found to be $\tau=3.8$. The grid resolution for simulations using the dynamic LANS-$\alpha$ equations and the LANS-$\alpha$ equations with fixed $\alpha$ is $64^3$, while the DNS data are performed at a grid resolution of $128^3$ before dealiasing.

Figure 6 shows the evolution of $\alpha$ for $\beta=0.8$ and 1.0. Similar to the decaying turbulence, a sharp decrease in the value of $\alpha$ is observed over the first eddy turn over time, where the values of $\alpha$ settle down toward a constant value. This corresponds to a statistically equilibrated state. As expected, the final value of $\alpha$ is in the inertial range of the energy spectrum.

Figure 7 shows the energy spectrum at $t=5.8\tau$ for $\beta=0.8$ and 1.0. An inertial subrange with $\sim k^{-5/3}$ energy spectrum is evident in the dynamic LANS-$\alpha$ simulations. The results of the dynamic LANS-$\alpha$ simulations are compared with the DNS and the LANS-$\alpha$ simulations with $\alpha=0.2$. The energy spectra of the dynamic LANS-$\alpha$ simulations for $\beta=0.8$ and 1.0 show a better agreement with the DNS data than the energy spectra for a LANS-$\alpha$ simulation with a constant $\alpha$.

### C. *A priori* test of a turbulent channel flow

*A priori* test of the dynamic LANS-$\alpha$ model is carried out in order to determine the accuracy of the model in predicting the SGS stresses and the energy dissipation rates in a wall-bounded flow. The tests are performed on the DNS data of del Álamo and Jiménez[25] for a turbulent channel flow. The turbulence Reynolds number, based on the wall friction velocity, is $\mathrm{Re}_\tau=550$ and the computational grid is $1536\times257\times1536$ in the streamwise, wall normal, and spanwise

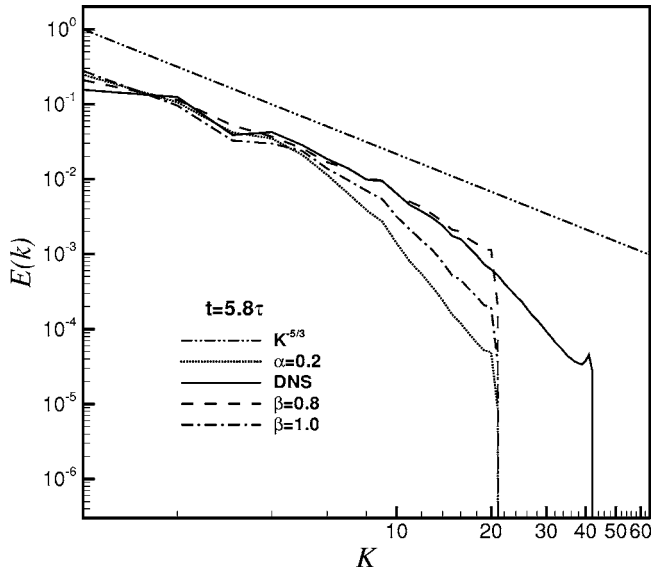


FIG. 7. Energy spectra at $t=5.8\tau$ for the DNS, dynamic LANS-$\alpha$, and LANS-$\alpha$ with fixed $\alpha$ simulations of a forced isotropic turbulence with $\mathrm{Re}_\lambda=415$ and $\tau=3.8$.

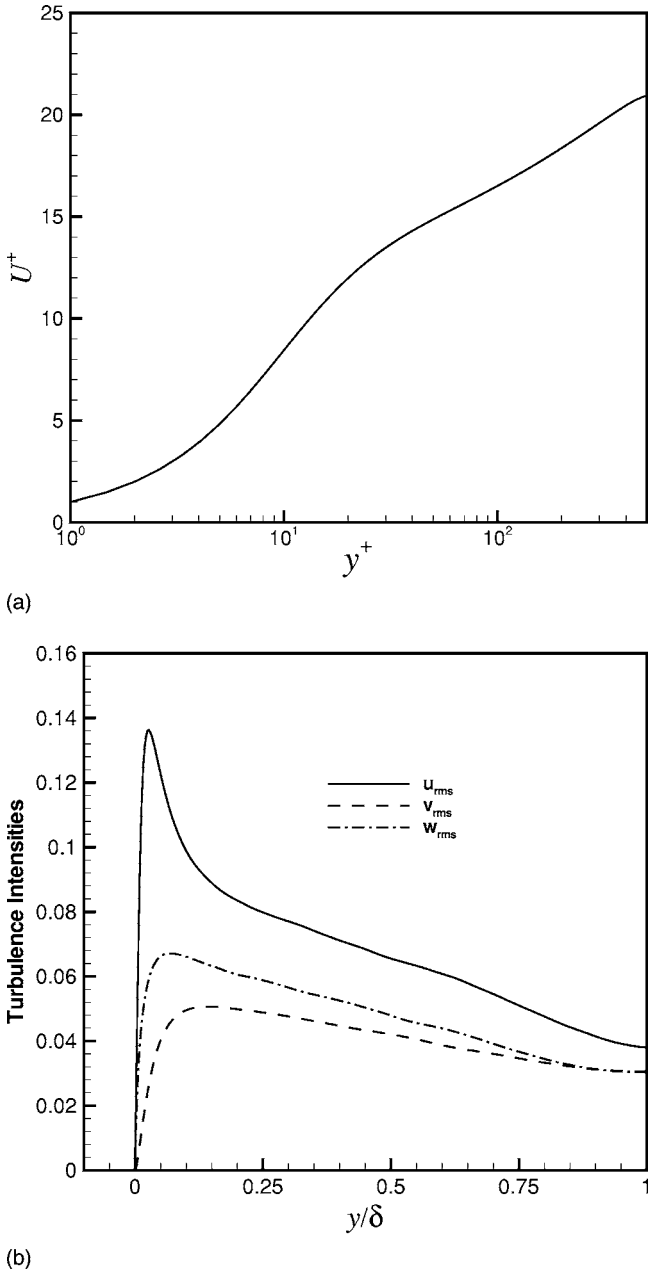


FIG. 8. DNS results of a turbulent channel flow at $\mathrm{Re}_\tau=550$ from del Álamo and Jiménez (Ref. 25). (a) The mean velocity profile and (b) root-mean-square velocity fluctuations in global coordinates.

directions, respectively. After dealiasing the physically relevant part of the computational domain reduces to $1024\times257\times1023$. The mean velocity profile, nondimensionalized by the wall-shear velocity, is depicted in Fig. 8(a), where a log layer from $y^+\approx80$ to 220 is observed. Figure 8(b) shows the turbulence intensity profiles from the wall to the middle of the channel in global coordinate which is normalized by half-channel height $\delta$. Maximum turbulence intensities in all directions are located in the wall layer.

Figure 9 shows the variation of $\alpha$ with the distance from the wall in both global and wall coordinates for $\beta=1.0$. As demonstrated in Fig. 9(b), $\alpha$ values experience a sharp increase in the vicinity of the wall up to $y^+=10$. This region of sharp increase in the value of $\alpha$ contains viscous sublayer. Diminishing values of $\alpha$ is observed as one approaches the wall. This is consistent with theoretical expectations that the NS equations ought to be recovered in the laminar layer at the wall. Away from the wall and beyond $y^+=10$, $\alpha$ shows some oscillations across the channel. Since the small variation of $\alpha$ value in the middle of the channel has little influence on the SGS stresses, one can argue that the dynamic LANS-$\alpha$ equations in this case divide the flow into two distinct regions: a near-wall region that includes the viscous sublayer where $\alpha$ is a function of distance from the wall and a constant $\alpha$ region which includes the buffer layer, log layer, and the outer layer. In the near-wall region, $\alpha$ holds an almost linear relation with the distance from the wall measured in wall units. Therefore, in wall-bounded flows, the isotropic LANS-$\alpha$ calculations could be used with a constant $\alpha$ beyond $y^+=10$ and with a linear function in the near-wall region. This projection requires further investigation in the LANS-$\alpha$ calculations.

Similar to the dynamic LES, one expects that the accuracy of the dynamic LANS-$\alpha$ model depends on its capability of accurately modeling the SGS stresses. The modeled and the exact SGS stresses in this flow are shown in Fig. 10 for the shear stress component $\langle\tau_{12}\rangle$, where $\langle\cdot\rangle$ stands for averaging in streamwise and spanwise directions. The general trend of the SGS stresses is captured in the dynamic LANS-$\alpha$ model without any *ad hoc* damping function even though the dynamic model underestimates the shear component of the SGS stresses. The SGS stresses vanish at the wall and in the middle of the channel with a maximum value within the wall layer. The dynamic LANS-$\alpha$ model is also compared with original LANS-$\alpha$ model with a fixed $\alpha=0.02$ in Fig. 10. It is seen that with a fixed $\alpha$ value, the LANS-$\alpha$ model cannot capture the correct SGS stress trend in the near-wall region. The exact and modeled dissipations $\langle\varepsilon_{\mathrm{SGS}}\rangle$ are compared in Fig. 11, where the averaged dissipa-

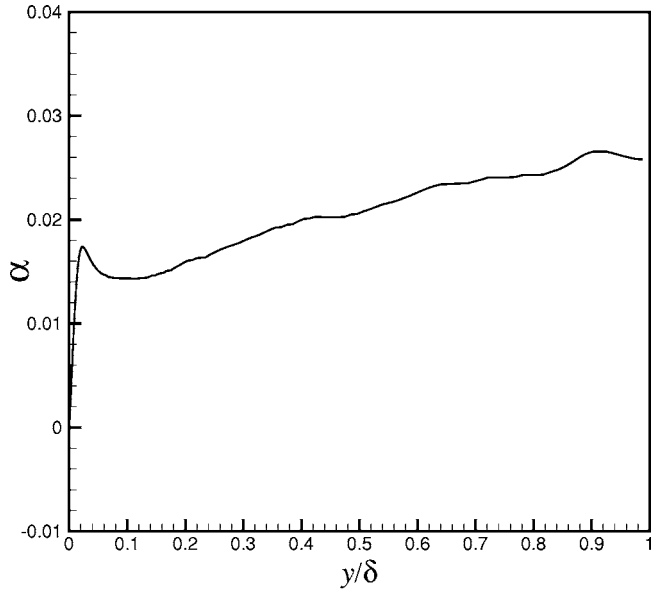


(a)

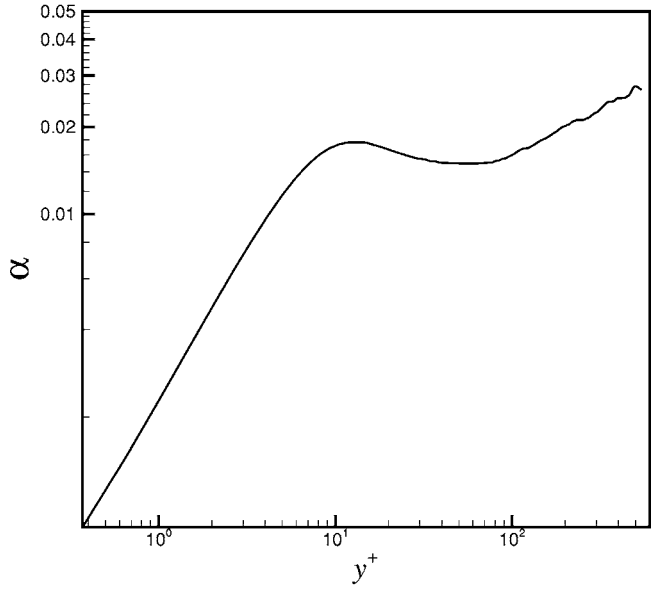


(b)

FIG. 9. Variation of $\alpha$ with distance from the wall in (a) global and (b) wall units.

tion is captured accurately by the dynamic LANS-$\alpha$ model in the near-wall region.

## VI. CONCLUSIONS

A dynamic LANS-$\alpha$ model is proposed where the variation in the parameter $\alpha$ in the direction of anisotropy is determined in a self-consistent way from the data contained in the simulation itself. The model results in a nonlinear equation for $\alpha$. Numerical experiments for decaying and forced homogenous isotropic turbulence are performed using the dynamic LANS-$\alpha$ model. The simulation results in both cases show an improvement over the LANS-$\alpha$ simulations with a fixed $\alpha$.

*A priori* test of the dynamic LANS-$\alpha$ model in a channel flow is carried out, where good agreement between the dynamic LANS-$\alpha$ predictions and the DNS data is observed. The parameter $\alpha$ is found to rapidly change in the wall normal direction in the vicinity of the wall. Near the solid wall, the length scale $\alpha$ shows a linear dependence on the wall normal direction in wall units. Away from the wall, and in the middle of the channel, the variation of $\alpha$ value is insignificant and $\alpha$ can be regarded as almost constant. As a result, the turbulent flow is divided into two regions: a constant $\alpha$ region away from the wall and a near-wall region. In the near-wall region, $\alpha$ holds an almost linear relationship with the distance from the wall. Consequently, one can argue that in wall-bounded flows, the isotropic LANS-$\alpha$ calculations could be used with a constant $\alpha$ beyond $y^+=10$ and with a linear function in the near-wall region. These results indicate

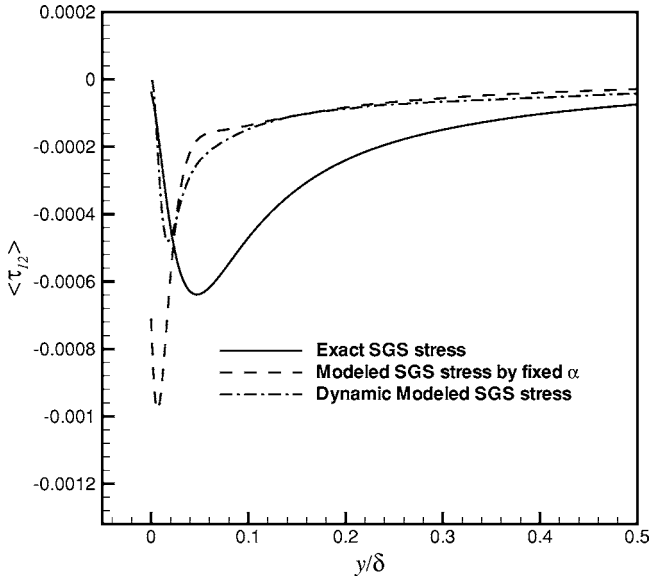


FIG. 10. The averaged subgrid-scale shear stress $\langle \tau_{12} \rangle$ in global units.

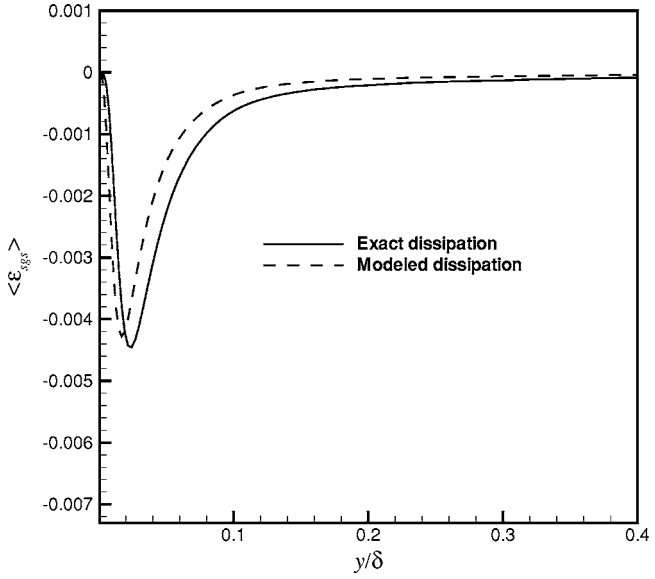


FIG. 11. The averaged dissipation in global units.

a promising application of the dynamic LANS-$\alpha$ model in wall-bounded turbulent flow simulations.

## ACKNOWLEDGMENTS

The research in this paper was partially supported by the AFOSR Contract Nos. F49620-02-1-0176 and FA9550-05-1-0334. The authors would like to thank B. Kosovic for his initial help in the derivation of the dynamic model and T. Lund and J.E. Marsden for helpful discussions. The DNS data of the channel flow was generously provided by R. Moser and J. Jiménez.

[1] D. Wilcox, *Turbulence Modeling for CFD* (DCW Industries, La Canada, CA, 1993).
[2] D. Holm, J. Marsden, and T. Ratiu, "Euler-Poincaré models of ideal fluids with nonlinear dispersion," Phys. Rev. Lett. **349**, 4173 (1998).
[3] H. S. Bhat, R. C. Fetecau, J. E. Marsden, K. Mohseni, and M. West, "Lagrangian averaging for compressible fluids," Multiscale Model. Simul. **3**, 818 (2005).
[4] J. Marsden and T. Ratiu, *Introduction to Mechanics and Symmetry*, 2nd ed. (Springer, New York, 1998).
[5] D. Holm, J. Marsden, and T. Ratiu *The Mathematics of Atmosphere and Ocean Dynamics* (Isaac Newton Institute, 1998).
[6] D. Holm, "Fluctuation effects on 3D Lagrangian mean and Eulerian mean fluid motion," Physica D **133**, 215 (1999).
[7] S. Chen, D. Holm, L. Margoin, and R. Zhang, "Direct numerical simulations of the Navier-Stokes-*alpha* model," Physica D **133**, 66 (1999).
[8] K. Mohseni, B. Kosović, S. Shkoller, and J. Marsden, "Numerical simulations of the Lagrangian averaged Navier-Stokes (LANS-$\alpha$) equations for homogeneous isotropic turbulence," Phys. Fluids **15**, 524 (2003).
[9] S. Chen, C. Foias, D. Holm, E. Olson, E. Titi, and S. Wynne, "Camassa-Holm equations as a closure model for turbulent channel and pipe flow," Phys. Rev. Lett. **81**, 5338 (1998).
[10] J. Marsden and S. Shkoller, "The anisotropic Lagrangian averaged Euler and Navier-Stokes equations,"Arch. Ration. Mech. Anal. **166**, 27 (2002).
[11] M. Germano, U. Piomelli, P. Moin, and W. Cabot, "A dynamic subgrid scale eddy viscosity model," Phys. Fluids A **3**, 1760 (1991).
[12] S. Ghosal, T. Lund, P. Moin, and K. Akselvoll, "A dynamic localization model for large-eddy simulation of turbulent flows," J. Fluid Mech. **285**, 229 (1995).
[13] C. Meneveau and T. Lund, "The dynamic Smagorinsky model and scale-dependent coefficients in the viscous range of turbulence," Phys. Fluids **9**, 3932 (1997).
[14] H. G. Im, T. S. Lund, and J. H. Ferziger, "Large eddy simulation of turbulent front propagation with dynamic subgrid models," Phys. Fluids **9**, 3826 (1997).
[15] V. Arnold, "Sur la géométrie différentielle des groupes de Lie de dimension infinie et ses applications à l'hydrodynamique des fluides parfaits," Ann. Inst. Fourier **16**, 319 (1966).
[16] H. Abarbanel, D. Holm, J. Marsden, and T. Ratiu, "Nonlinear stability of stratified flow," Phys. Rev. Lett. **52**, 2352 (1984).
[17] C. Kane, J. Marsden, M. Ortiz, and M. West, "Integrators and the newmark algorithm for conservative and dissipative mechanical systems," Int. J. Numer. Methods Eng. **49**, 1295 (2000).
[18] A. Lew, J. Marsden, M. Ortiz, and M. West, "Asynchronous variational integrators," Arch. Ration. Mech. Anal. **167**, 85 (2003).
[19] A. Chorin and J. Marsden, *A Mathematical Introduction to Fluid Mechanics*, 3rd ed. (Springer, New York, 1994).
[20] K. Mohseni, "Statistical equilibrium theory of axisymmetric flows: Kelvin's variational principle and an explanation for the vortex ring pinch-off process," Phys. Fluids **13**, 1924 (2001).
[21] C. Lim, "A long range spherical model and exact solutions of an energy enstrophy theory for two-dimensional turbulence," Phys. Fluids **13**, 1961 (2001).
[22] R. Ellis, K. Haven, and B. Turkington, "Nonequivalent statistical equilibrium ensembles and refined stability theorems for most probable flows," Nonlinearity **15**, 239 (2002).
[23] A. Majda and M. Holen, "Dissipation, topography and statistical theories for large-scale coherent structure," Commun. Pure Appl. Math. **50**, 1183 (1997).
[24] D. Lilly, "A proposed modification of the Germano subgrid-scale closure method," Phys. Fluids A **4**, 633 (1992).
[25] J. del Álamo and J. Jiménez, "Spectra of the very large anisotropic scales in turbulent channels," Phys. Fluids **15**, L41 (2003).
[26] J. Kim, P. Moin, and R. Moser, "Turbulence statistics in fully developed channel flow at low Reynolds number," J. Fluid Mech. **177**, 133 (1987).
[27] R. Moser, J. Kim, and N. Mansour, "Direct numerical simulation of turbulent flow up to $Re_\tau$=590," Phys. Fluids **11**, 943 (1999).